

Interface suppressed nematicity and enhanced superconductivity of FeSe/NdFeO₃ in the low doping regime

Chihao Li,¹ Yuanhe Song,¹ Xiaoxiao Wang,¹ Minyinan Lei,¹ Xiaoyang Chen,¹ Haichao Xu,^{1,2,*} Rui Peng,^{1,2,†} and Donglai Feng^{1,3,4,5,‡}

¹Laboratory of Advanced Materials, State Key Laboratory of Surface Physics, and Department of Physics, Fudan University, Shanghai 200438, China

²Shanghai Research Center for Quantum Sciences, Shanghai 201315, China

³National Synchrotron Radiation Laboratory and School of Nuclear Science and Technology, University of Science and Technology of China, Hefei, 230026, China

⁴New Cornerstone Science Laboratory, University of Science and Technology of China, Hefei, 230026, China

⁵Collaborative Innovation Center of Advanced Microstructures, Nanjing 210093, China

(Dated: July 17, 2024)

The discovery of interface-enhanced superconductivity in single-layer FeSe/oxides has generated intensive research interests. Beyond the family of FeSe interfaced with various TiO₂ terminated oxides, high pairing temperature up to 80 K has been recently observed in FeSe interfaced with FeO_x-terminated LaFeO₃. Here we successfully extend the FeSe/FeO_x superconducting interface to FeSe/NdFeO₃, by constructing 1uc-FeSe/6uc-NdFeO₃/Nb:SrTiO₃ heterostructures. Intriguingly, well-annealed FeSe/NdFeO₃ exhibits a low doping level of 0.038~0.046 e⁻/Fe which deviates universally magic doping level (0.10~0.12 e⁻/Fe) and provides a new playground for studying the FeSe/oxide interface in the low electron-doped regime. Comparing it with thick FeSe films at the comparable electron doping level induced by surface potassium dosing, FeSe/NdFeO₃ shows a larger superconducting gap and the absence of a nematic gap, indicating an enhancement of the superconductivity and suppression of nematicity by the FeSe/FeO_x interface. These results not only expand the FeSe/FeO_x superconducting family but also enrich the current understanding on the roles of the oxide interface.

I. Introduction

The discovery of high-temperature interfacial superconductivity in one unit cell (1uc) FeSe/SrTiO₃ [42] has ignited intensive research interests. The superconducting pairing temperature in 1uc FeSe/SrTiO₃ ($T_g \sim 65\text{K}$) [10, 39] exhibits a substantial enhancement compared to that of bulk FeSe crystals (superconducting critical temperature $T_c \sim 8\text{K}$) [13]. Interface engineering on the epitaxial strain, charge transfer, and interfacial electron-phonon coupling have been conducted [7, 18, 28, 29, 32, 34, 36, 40, 44, 46, 47], revealing the significant contributions of interface charge transfer and interfacial electron-phonon coupling to the enhancement of superconducting pairing [7, 18, 32, 36, 40, 46, 47].

To examine the generality of the mechanism underlying the enhancement of interfacial superconductivity and to explore new interfacial superconductors, it is crucial to investigate FeSe films interfaced with other oxides. Extending the superconducting interfaces, a range of FeSe interfaces with TiO_x-terminated oxides has been explored. These include 1uc FeSe on BaTiO₃ [29], on anatase TiO₂ (001) [6], on rutile TiO₂ (100) [32], SrTiO₃ (110) [46, 48, 52], on EuTiO₃ [22] and on LaTiO₃ [14]. Angle-resolved photoemission spectroscopy (ARPES) measurements have revealed that well-annealed 1uc FeSe on different TiO_x-terminated interfaces generally exhibit substantial electron doping (0.10~0.12 e⁻/Fe), referred as “magic doping” [14, 19]). It puts 1 uc

FeSe/titanate at the heavy electron doping regime of the phase diagram, where nematicity is absent [28, 29, 39, 44, 50]. Moreover, replica bands reflecting the interfacial electron-phonon coupling are commonly observed in these FeSe-oxide interfaces [7, 18, 20, 32, 46]. However, it remains challenging to construct new types of FeSe/oxide interfaces beyond the FeSe/TiO_x structure in order to test the generality of this mechanism.

Very recently, Song et. al reported the successful fabrication of high-quality monolayer FeSe films on the FeO_x-terminated LaFeO₃ [37], in which the superconducting pairing temperature reaches 80 K, surpassing the boiling temperature of nitrogen. This work suggests that a similar pairing enhancement mechanism operates at the FeSe/LaFeO₃ interface as observed in the FeSe/TiO_x-terminated interfaces [37]. Yet, the FeSe/LaFeO₃ interface remains the only reported instance of the FeSe/FeO_x superconducting interface. Could it be possible to achieve epitaxial growth of 1uc-FeSe on other XFeO₃ (X=Nd, Pr, Bi, and etc.) perovskites? By expanding the FeSe/FeO_x family, we can potentially establish new platforms to explore the characters of FeSe-based interfacial superconductivity. In particular, it is worth noting that the reported FeSe/LaFeO₃ exhibits a lower electron doping (0.087 e⁻/Fe) compared to the magic doping observed in FeSe/TiO_x-terminated interfaces. By studying FeSe on various XFeO₃ substrates, valuable insights can be gained into the FeSe/oxide interface under doping conditions that differ from FeSe/titanates.

Here we have successfully fabricated a new high-quality FeSe/FeO_x interface by growing a 1uc FeSe film on a 6uc epitaxially grown NdFeO₃ layers on Nb:SrTiO₃ substrates. Through in-situ ARPES measurements, we have determined that the electron doping level of the well-annealed

* xuhaichao@fudan.edu.cn

† pengrui@fudan.edu.cn

‡ dlffeng@ustc.edu.cn

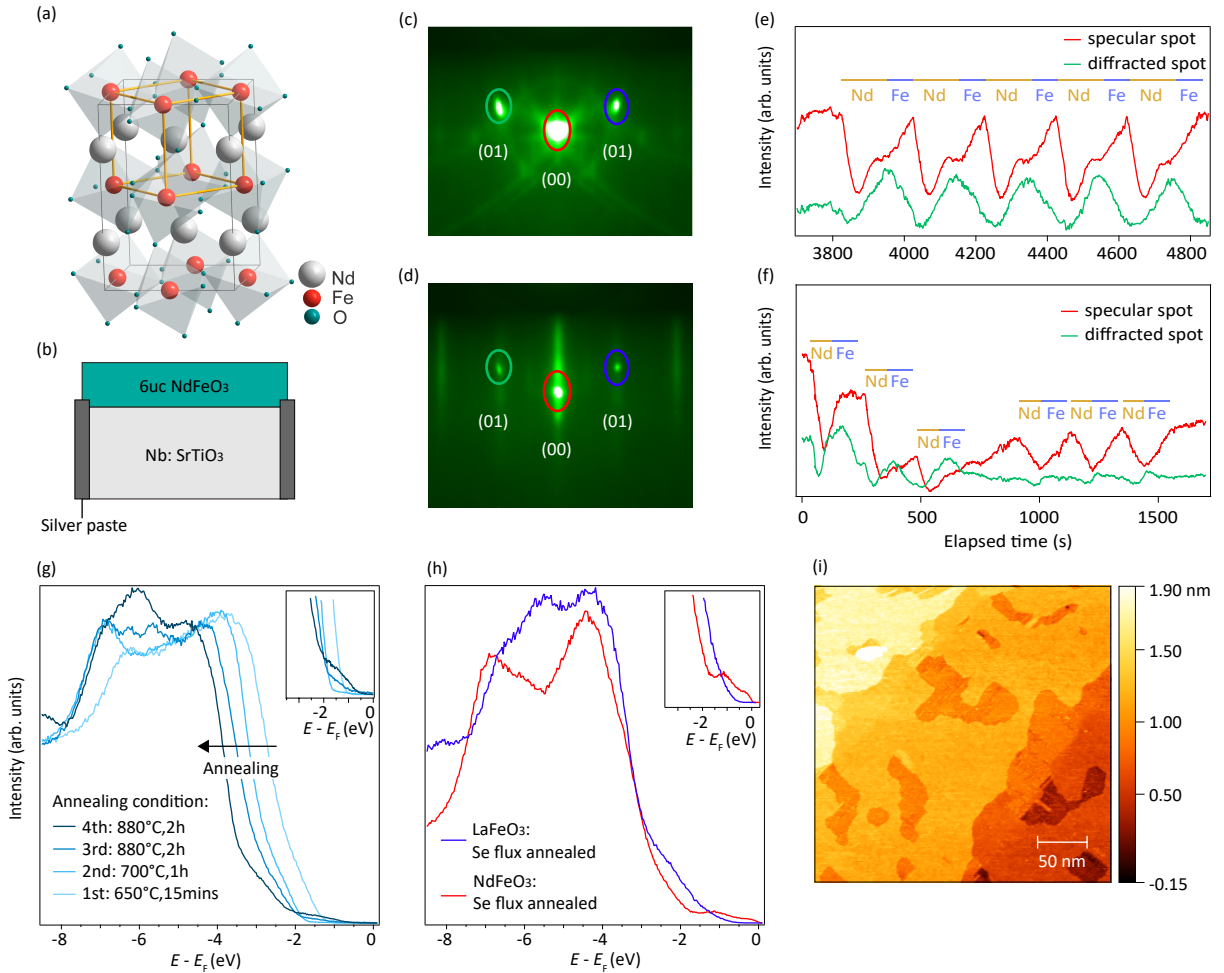


FIG. 1. (a) Crystal structure of NdFeO_3 . (b) Schematic illustration of the heterostructure. (c) Reflection high-energy electron diffraction (RHEED) pattern of the annealed Nb:SrTiO_3 substrates, showing sharp Kikuchi lines. (d) RHEED pattern of the epitaxial 6uc NdFeO_3 films, showing two-dimensional RHEED streaks. (e) The intensity oscillation of the diffracted and specular RHEED spots during the growth of a calibration sample. (f) The intensity oscillation of the diffracted and specular RHEED spots during the growth of the 6uc NdFeO_3 . (g) Valence band comparison of the $6\text{uc NdFeO}_{3-\delta}/\text{Nb:SrTiO}_3$ film after each annealing experiment. The valence bands shift to higher binding energy with longer annealing times, suggesting increasing electron doping due to oxygen vacancies. (h) Valence band comparison between Se flux-annealed $6\text{-uc NdFeO}_{3-\delta}/\text{Nb:SrTiO}_3$ and Se flux-annealed $6\text{-uc LaFeO}_3/\text{Nb:SrTiO}_3$ [37]. They exhibit comparable oxygen vacancy density as indicated by the valence band position. (i) Scanning Tunneling Microscopy (STM) image of the annealed $6\text{uc-NdFeO}_3/\text{Nb:SrTiO}_3$.

$1\text{uc FeSe}/\text{NdFeO}_3/\text{Nb:SrTiO}_3$ interface is only $0.038\sim 0.046 e^-/\text{Fe}$, which is lower than the doping levels observed in the various 1uc FeSe on TiO_x -terminated oxides ($0.10\sim 0.12e^-/\text{Fe}$) [6, 14, 22, 28, 29, 32, 39] and in $\text{FeSe}/\text{LaFeO}_3$ ($0.087 e^-/\text{Fe}$) interfaces [37], placing the superconducting interface of $\text{FeSe}/\text{NdFeO}_3$ in the low doping regime of electron-doped FeSe phase diagram. Compared to FeSe thick films with similar levels of electron doping [35, 44, 50], the $\text{FeSe}/\text{NdFeO}_3$ system exhibit an enhancement of superconductivity and the suppression of nematic splitting. This observation suggests that the FeSe/FeO_x interface plays an additional role beyond the electron doping. Our findings not only extend the FeSe/FeO_x superconducting family, but also provide evidence for the tailored band structure achieved through the interface, shedding light on the intricate interplay between interfacial superconductivity and nematicity.

II. MBE growth of $1\text{uc FeSe}/6\text{uc NdFeO}_3/\text{Nb:SrTiO}_3$

NdFeO_3 (NFO) bulk crystals exhibit a structurally distorted perovskite structure with lattice constants of $a=5.450 \text{ \AA}$, $b=5.587 \text{ \AA}$, $c=7.761 \text{ \AA}$ [Fig. 1(a)] [17]. The pseudo-cubic lattice constant of NFO is $a'=3.895 \text{ \AA}$ and the lattice mismatch with SrTiO_3 substrate is only -0.25% . Commercial TiO_x terminated 0.5% wt Nb -doped $\text{SrTiO}_3(001)$ substrates (NSTO) with $0.1^\circ \sim 0.15^\circ$ miscut angle (CrysTec) were used as substrates. The NSTO substrates were annealed at 500°C in the molecular beam epitaxy (MBE) chamber (base vacuum 7×10^{-10} mbar) for 1 hour, using an pressure of 2×10^{-7} mbar under ozone atmosphere. The RHEED pattern of the annealed NSTO substrates shows sharp Kikuchi lines [Fig. 1(c)]. Subsequently, NFO films were grown on the annealed substrates by ozone-assisted molecular beam epitaxy at 650°C

with pressure of 2×10^{-7} mbar under ozone atmosphere. By alternately opening the pneumatic shutters of the Nd source and the Fe source, the oxidized Nd and Fe layers were alternately grown on the substrate in an atomic layer-by-layer mode. The relative stoichiometry and the absolute amount of each element (La and Fe) was first calibrated by quartz crystal microbalance (QCM) measurements and then by real-time intensity oscillations of reflection high-energy electron diffraction (RHEED) during the growth [9, 28, 29]. After calibration, stable oscillations of RHEED intensity can be obtained, indicating a stoichiometric Nd-Fe atomic flux ratio [Fig. 1 (e)]. Subsequently, 6 uc NdFeO₃ films were grown on freshly-annealed Nb:SrTiO₃ substrates following the calibrated stoichiometry [Fig. 1(f)]. The RHEED streaks suggest two-dimensional growth character of the grown NdFeO₃ films [Fig. 1(d)]. Using this atomic layer-by-layer epitaxial growth method, we control NdFeO₃ to be FeO_x-terminated.

Oxygen vacancies in the substrates are vital for epitaxially growing high-quality FeSe films [6, 8, 14, 22, 27, 32, 36, 39, 42, 46, 48, 52]. To induce sufficient oxygen vacancies, the NdFeO₃ films were annealed four times under vacuum, and the valence bands were examined using ARPES after each annealing step. As shown in Fig. 1(g), the valence bands (VB) of NdFeO_{3- δ} /Nb:SrTiO₃ shift towards higher binding energy upon vacuum annealing, suggesting increasing electron doping with increasing oxygen vacancies. In contrast to the wide insulating band gap observed in NdFeO₃, an increase in the density of states near the Fermi level is observed in NdFeO_{3- δ} films with higher oxygen vacancy densities resulting from stronger annealing conditions. This observation suggests the presence of low-energy states induced by oxygen vacancies [1, 4, 12, 23, 39]. Subsequently, the NdFeO_{3- δ} /Nb:SrTiO₃ films were transferred to a Chalcogenide-MBE chamber and annealed under Se flux at 950 °C for 45 minutes. After the annealing, the valence band peaks of the NdFeO₃ films at 4 eV below the Fermi energy are similar to those of the annealed LaFeO₃ films under Se flux, suggesting comparable oxygen vacancy densities [see Fig. 1(h)]. Note that the annealed NdFeO_{3- δ} films exhibit a higher spectral weight near the Fermi level [see Fig. 1(g-h)], when compared to LaFeO_{3- δ} [37]. This observation indicates that the concentration of oxygen vacancies in the surface layers of NdFeO₃ is no less than that in LaFeO₃.

The topography measurements were performed by a scanning tunneling microscope [STM, (RHK Technology)] that in-situ connected with the ARPES chamber and MBE chambers in the combined ultra-high vacuum (UHV) system. The samples were measured at 17 K under pressure of $\sim 1 \times 10^{-10}$ mbar. The annealed NdFeO₃/Nb:SrTiO₃ films exhibit atomically flat surfaces, as observed by in-situ scanning tunneling microscopy (STM) in Fig. 1(i). Subsequently, 1uc FeSe films were grown on the NdFeO₃/Nb:SrTiO₃ heterostructures at a temperature of 490 °C, using a Fe/Se flux rate ratio of 1:10, followed by annealing at 520 °C for 3 hours. The STM morphology image of the annealed 1uc FeSe/NdFeO₃/Nb:SrTiO₃ [Fig. 2(b)] exhibits well-defined terrace edges, predominantly 1uc in thickness with a few 2 uc areas [Supplementary Fig. S2].

III. Low electron doping in 1uc FeSe/6uc NdFeO₃/Nb:SrTiO₃

In-situ angle-resolved photoemission spectroscopy (ARPES) studies were performed on the grown 1uc-FeSe/6uc-NdFeO₃/Nb:SrTiO₃ (hereafter referred as FeSe/NFO) with the 21.2eV(He-I α) helium discharge lamp from Fermi Instrument and the VG-Scienta DA30 electron analyzer, under the ultra-high vacuum better than 2.5×10^{-11} mbar. All ARPES measurements were conducted at 9K. The energy resolution is 6 meV and the angular resolution is 0.3°. Around the Γ point, a parabolic band denoted as α band was observed, with its band top locate at 45 meV below the Fermi energy [Fig. 2(d)], which is higher than that of FeSe/SrTiO₃ of 80 meV below the Fermi energy and FeSe/LaFeO₃ of 70 meV below the Fermi energy, suggesting that the electron doping level of the FeSe/NdFeO₃ interface is lower than that in FeSe/SrTiO₃ interface and FeSe/LaFeO₃ interface.

Figure 2(e) shows the measured band structure near the M point, where two electron bands, labeled as γ_1 and γ_2 . The electron bands γ_1 and γ_2 can be further identified by extracted momentum distribution curves (MDCs) and fitted bands according to peak positions of MDCs [Fig. 2(f-g)]. The sizes of the semi-minor axis (k_1) and the semi-major axis (k_2) of the elliptical Fermi pocket were determined to be 0.096 \AA^{-1} and 0.172 \AA^{-1} , respectively. According to Luttinger's theorem, the electron doping level of the FeSe/NFO interface, derived from the Fermi surface volume, is $0.040 e^-/\text{Fe}$, which is lower than that of 1uc FeSe/SrTiO₃ interface ($0.10 \sim 0.12 e^-/\text{Fe}$) and 1uc FeSe/LaFeO₃ interface ($0.087 e^-/\text{Fe}$). To confirm this, experiments were repeated on a series of 1uc FeSe/NdFeO₃/Nb:SrTiO₃ samples, and the electron doping level ranged from $0.038 e^-/\text{Fe}$ to $0.046 e^-/\text{Fe}$ (refer to supplementary Fig. S3), indicating a consistently low doping level at the FeSe/NFO interface. The band structure of the FeSe/NFO is similar to that of the FeSe/SrTiO₃ and FeSe/LaFeO₃ interfaces, except for a downward shift in the chemical potential [37, 39].

Such a low electron doping level of 1uc FeSe/NdFeO₃ falls within the underdoped region of electron-doped FeSe [44], suggesting that the charge transfer effect at the FeSe/NdFeO₃ interface is weaker compared to that of FeSe/SrTiO₃ and FeSe/LaFeO₃, despite the presence of an similar quantity of oxygen vacancies as suggested by the valence band structure in Fig. 1(h).

IV. Suppressed nematicity in 1uc FeSe/6uc NdFeO₃/Nb:SrTiO₃

Figure 3 shows the band structure of a surface potassium(K)-doped FeSe sample and the FeSe/NdFeO₃ samples in comparable doping levels. Around M, for K-doped FeSe, the band bottom of γ_2 is at E_F -65 meV and the band bottom of γ_1 is at E_F -35 meV, showing a 30 meV splitting of the band bottoms at M [Fig. 3(a,c)]. In contrast, by fitting the peak positions of the MDCs to a parabolic dispersion, we find that the band γ_1 and the band γ_2 of FeSe/NdFeO₃ samples exhibit the same band bottom at E_F -34 meV, without splitting

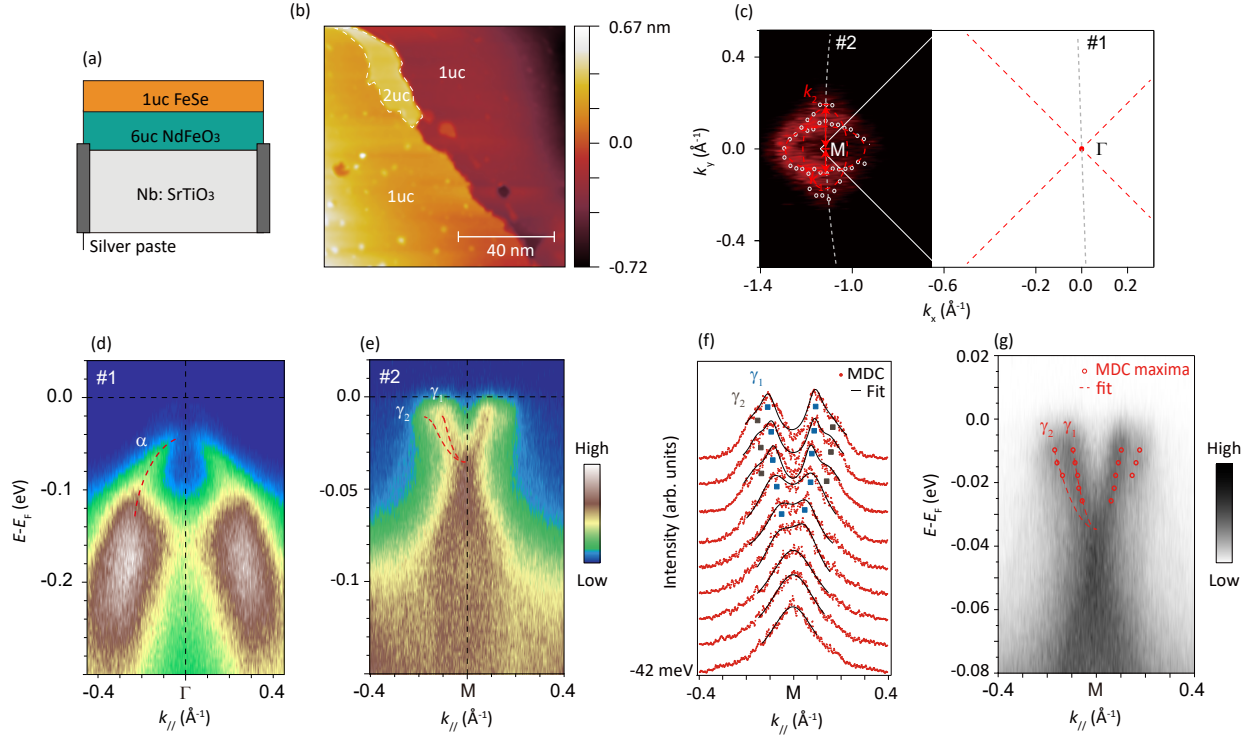


FIG. 2. (a) Structure of 1uc-FeSe/6uc-NdFeO₃/Nb:SrTiO₃. (b) STM morphology of annealed 1uc-FeSe/6uc-NdFeO₃/Nb:SrTiO₃. (c) Fermi surface of 1uc-FeSe/6uc-NdFeO₃/Nb:SrTiO₃ heterostructure. Open circles refer to fitted k_F from in-plane mappings (cut by cut) and the grey elliptical circle refer to 2 non-degenerate electron pockets at the M point, suggesting relatively low electron doping level. (d) Band dispersion near Γ point along the cut #1 shown in Fig (c). The hole band of FeSe is labeled as α . (e) Band dispersion near M point along the cut #2 shown in Fig (c), labeling the 2 electron bands as γ_1 and γ_2 . (f) MDC near the M point. The FeSe/ NdFeO₃ exhibits non-degenerate electron pockets at the Fermi level. (g) Fitted electron bands plotted on the band dispersion along the cut #1 shown in Fig (c). All the ARPES measurements were conducted at 9K.

[Fig. 3(b,d)]. Around Γ , for K-doped FeSe films [Fig.3(d)], there is one hole band crossing the Fermi level from the undoped FeSe underlayer, while the topmost doped FeSe shows two hole bands with the band top located at E_F-10 meV for the band most close to the Fermi level [44]. However, for FeSe/NdFeO₃, the top of hole band at the Γ point is located further below the Fermi level (E_F-45 meV), which is the character of 1uc FeSe/oxides [Fig. 3(e)]. Therefore, there is a stark contrast in the band structure between 1 uc FeSe/NdFeO₃ and K-doped FeSe thick films with comparable electron doping levels ($0.040 e^-/\text{Fe}$ for FeSe/NdFeO₃ and $0.046 e^-/\text{Fe}$ for K-doped FeSe thick films [44]).

The splitting of bands γ_1 and γ_2 is commonly observed in FeSe bulk crystals [25, 45, 49], FeSe thick films [24, 39, 44] and underdoped K-doped FeSe [44] below the nematic transition temperature, representing different occupation between the d_{xz} and d_{yz} orbitals due to nematicity [3, 33]. The larger energy separation of the bands reflects the stronger strength of the nematic order [39]. Here the negligible energy separation in 1 uc FeSe/NdFeO₃ suggests an absence of nematicity. It should be noted that such doping corresponding to a nematic regime in thick FeSe films [44], and thus the interface plays intriguing roles in varying the band structure and suppressing nematicity beyond simple electron doping.

V. Superconducting gap and phase diagram

Figure 4(a) presents the symmetrized photoemission spectrum of 1uc-FeSe/6uc-NdFeO₃/Nb:SrTiO₃ measured at 9 K at the M point. The observed back-bending behavior is a hallmark of Bogliubov quasiparticle dispersion, and a superconducting gap opening is observed. Figure 4(b) and Fig. 4(c) show the energy distribution curve (EDC) and corresponding fits for the superconducting gap at two momentum positions. According to spectral function fitting, the superconducting gap sizes Δ at k_1 (the minor axis endpoint of the Fermi pocket at M point) and k_2 (the major axis endpoint of the Fermi pocket at M point) are 8.5 meV and 10.3 meV respectively. Furthermore, superconducting spectral function fitting provides insights into the single-particle scattering rate Γ_2 , which reflects the level of impurity scattering and the quality of the films. The single-particle scattering rate coefficient Γ_2 is 11.3 meV at k_2 (the outer elliptical electron pocket), which is similar to that of the high-quality 1uc FeSe/SrTiO₃ heterostructures ($\Gamma_2 = 12$ meV) [36], indicating that the 1uc FeSe/6uc NdFeO₃/Nb:SrTiO₃ samples are of good quality without strong impurity scattering. Note that the superconducting gap is absent in K-doped FeSe films with a comparable doping level [35, 44], suggesting that the origin of the

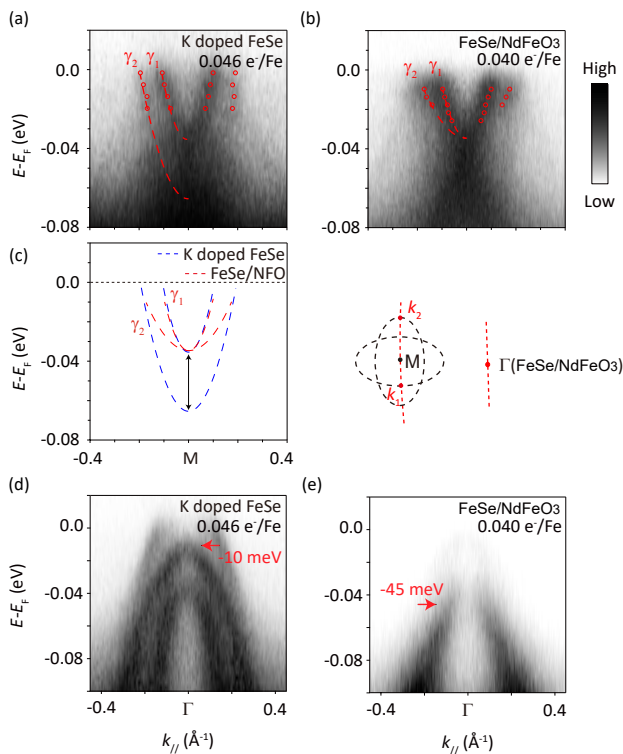


FIG. 3. Band dispersion and fitting at M point of different samples: (a) K-doped FeSe with the doping level of $0.046e^-/\text{Fe}$; (b) FeSe/NFO with doping level of $0.040e^-/\text{Fe}$. (c) Fitting comparison between K-doped FeSe and FeSe/NFO. (d) Band dispersion of FeSe/NFO at the Γ point; (e) Band dispersion of K-doped FeSe films at the Γ point. The band tops which do not cross the Fermi level are marked by red arrows.

enhanced superconductivity in FeSe/NdFeO₃ is beyond simple electron doping.

In Fig.4(d), we plot the energy scales of superconducting gap and nematic splitting in 1uc FeSe films interfaced with various FeO_x terminated oxides as a function of electron doping [37], together with those of the surface doped thick FeSe films [35, 44, 50] and well annealed 1uc FeSe/SrTiO₃ [7, 14, 22, 29, 32, 39]. For electron-doped FeSe without an oxide interface, the comparable electron doping level of FeSe/NdFeO₃ is close to the boundary of superconductivity and in a partially suppressed nematic order state [35, 44]. For 1uc FeSe/NdFeO₃ heterostructure, a superconducting pairing gap Δ of 10.3 meV is observed with no energy splitting at M point, suggesting that nematicity is suppressed while superconducting pairing strength is enhanced by the FeSe/NdFeO₃ interface.

VI. Discussion

Previous ARPES studies have revealed that for the 1uc FeSe/TiO_x interface, the doping level of 1uc FeSe films is pinned to $0.10\sim 0.12e^-/\text{Fe}$ (i.e. “magic doping”) [14, 19]. However, the well-annealed 1uc-FeSe/6uc-

NdFeO₃/Nb:SrTiO₃ samples have lower electron doping levels of $0.038\sim 0.046e^-/\text{Fe}$, deviating from the “magic doping”. Based on the VB shift and density of states (DOS) at E_F , it is evident that the density of oxygen vacancies is equal to or exceeds that in FeSe/LaFeO₃. Therefore, the NdFeO₃ acts as “infinite” charge reservoir, and the doping level of FeSe/NdFeO₃ is not constrained by oxygen vacancies but could potentially be limited by a smaller work function mismatch. This calls for future studies into the variations of work functions across different FeSe-FeO_x and FeSe-TiO_x interfaces.

FeSe/NdFeO₃ is the first well-annealed FeSe/oxide interface that exhibits low electron doping in 1uc FeSe films, which provides new insights into the role of the interface. It is shown that nematicity can be enhanced by tensile strain [21, 30, 39, 51]. Consequently, it is expected nematicity would be strongest in 1uc FeSe/STO with the strongest tensile strain if without interfacial electron transfer [39]. However, our results provide direct evidence that the nematicity is even weaker in 1uc FeSe/NdFeO₃ than the similarly doped thick FeSe with less tensile strain. Further theoretical development is required to elucidate the origin of the suppressed nematicity by the interface, while it is likely that the altered band structure of FeSe by the oxide interface plays some role. In iron-based superconductors, nested electron and hole pockets at the Fermi surface are suggested to induce strong spin fluctuation [11] and drive nematicity [43]. When the nesting conditions deteriorate, the nematic order is suppressed [26]. In comparison to K-doped thick FeSe with similar electron doping, the hole-like band of 1-uc FeSe/NdFeO₃ is far from the Fermi surface, and the significantly poorer nesting conditions may contribute to the suppression of nematicity.

The interaction between the electrons in FeSe and interfacial optical photons has been suggested to boost superconductivity in FeSe/STO and FeSe/LaFeO₃ [7, 36, 37]. There are two optical phonon modes in NdFeO₃ corresponding to the relative motion of Fe-O atoms within the oxygen octahedron of 55.8 meV and 79.8 meV, respectively [5]. The 79.8 meV optical phonon mode is similar in energy scale to the previously reported phonon modes in the FeSe/LaFeO₃ interface [37]. Although the data statistics of the EDC at M point are not high enough for replica band fitting, the integrated EDC shows a peak-dip-hump structure at M point, and the energy separation between the peak and hump is around 80 meV, supporting the coupling between electrons and the FK phonons of NdFeO₃ [36, 37] (Details can be seen in supplementary Fig.S5). Furthermore, given that FeSe/NdFeO₃ is closer to the nematic phase but lacks nematic order, it is intriguing to investigate whether nematic fluctuations play an additional role in enhancing superconductivity in the low electron-doped region, in addition to the cooperative effect of interfacial electron-phonon coupling (EPC).

To summarize, we have successfully grown FeSe/NdFeO₃ interface, and demonstrate it as a new member of the FeSe/FeO_x interfacial superconductor family. Note that there are multiple magnetic ordered states in NdFeO₃ [2, 15, 16, 31, 38, 41], and the extending of FeSe/FeO_x interfacial superconductor family provides a new platform to engineer and

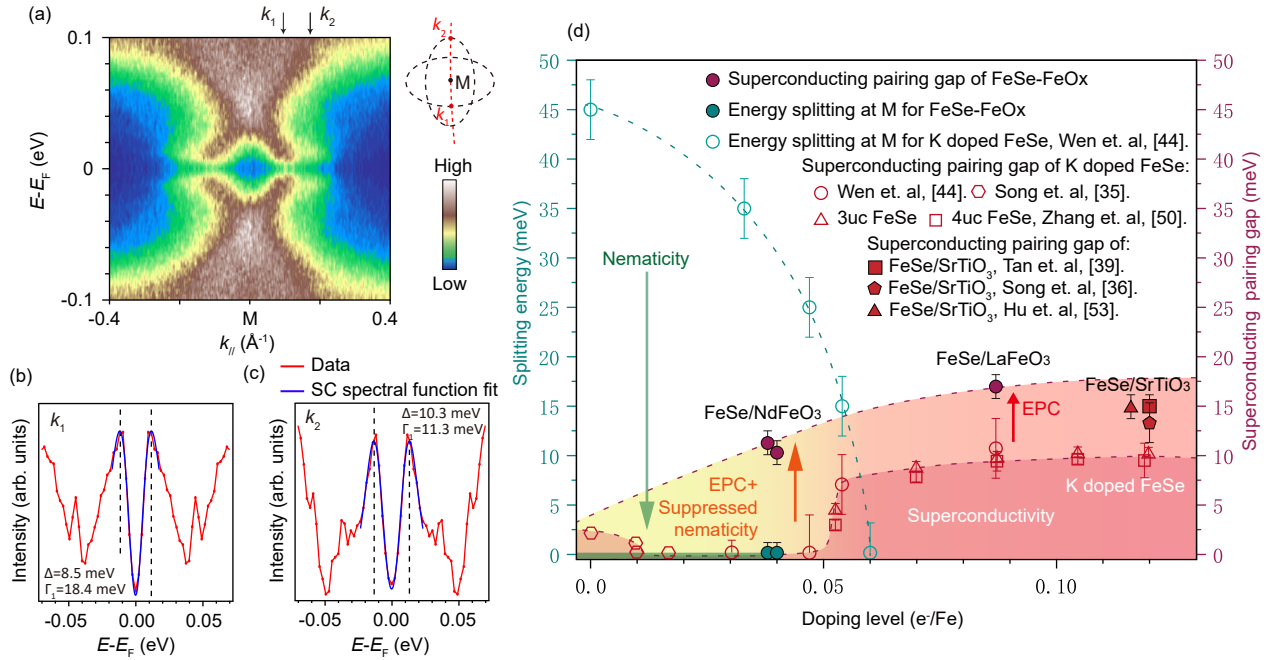


FIG. 4. (a) Symmetrized band dispersion of # 2 shown in Fig. 2(e), showing the superconducting pairing gap Δ . (b) Energy distribution curve at the momentum of k_1 shown in Fig (a) with the fitted superconducting pairing gap $\Delta_{k_1}=8.5$ meV and the single-particle scattering rate Γ_1 of 18.4 meV. (c) Energy distribution curve at the momentum of k_2 shown in Fig (a) with the fitted superconducting pairing gap $\Delta_{k_2}=10.3$ meV and the single-particle scattering rate $\Gamma_1 =11.3$ meV. All the ARPES measurements were taken at 9K. (d) Phase diagram of nematic order induced energy splitting and superconducting pairing gap for FeSe-FeO_x, FeSe/SrTiO₃ and K-doped FeSe against electron doping level. The solid-circle-shaped data refer to FeSe-FeO_x. The open-circle-shaped data refer to K-doped FeSe data adapted from ref. [44] (Wen et. al), the open-triangle-shaped data and the open-square-shaped data refer to K-doped FeSe data adapted from ref. [50] (Zhang et. al), the open-hexagon-shaped data refer to K-doped FeSe data adapted from ref. [35] (Song et. al), the solid-square-shaped data refer to well-annealed 1uc FeSe/SrTiO₃ data adapted from ref. [39] (Tan et. al), the solid-pentagon-shaped data refer to well-annealed 1uc FeSe/SrTiO₃ data adapted from ref. [36] (Song et. al) and the solid-triangle-shaped data refer to well-annealed 1uc FeSe/SrTiO₃ data adapted from ref. [53] (Hu et. al). FeSe-FeO_x interfaces exhibit superconducting pairing strength enhancement and nematicity suppression compared to K-doped FeSe.

study the interaction between superconductivity and magnetism. Moreover, the charge transfer of the interface can be controlled at the underdoped region ($0.038\sim 0.046 e^-/Fe$), which is the first underdoped case in the well-annealed 1uc FeSe/oxide family. The observed nematicity suppression provides new information in understanding the interaction between oxide interfaces and FeSe.

ACKNOWLEDGMENTS

This work is supported in part by the National Science Foundation of China under the grant Nos. 11922403,

12274085, 12074074 and 92365302, the National Key R&D Program of the MOST of China (2023YFA1406300), the New Cornerstone Science Foundation, the Innovation Program for Quantum Science and Technology (Grant No. 2021ZD0302803), and Shanghai Municipal Science and Technology Major Project (Grant No.2019SHZDZX01).

[1] Y Aiura, I Hase, H Bando, T Yasue, T Saitoh, and DS Dessau. Photoemission study of the metallic state of lightly electron-doped srtio3. *Surface Science*, 515(1):61–74, 2002.
 [2] J Bartolomé, E Palacios, MD Kuz’Min, F Bartolomé, I Sosnowska, R Przeniosło, R Sonntag, and MM Lukina. Single-crystal neutron diffraction study of nd magnetic ordering in nd-feo 3 at low temperature. *Physical Review B*, 55(17):11432,

1997.
 [3] Anna E Böhmer, Jiun-Haw Chu, Samuel Lederer, and Ming Yi. Nematicity and nematic fluctuations in iron-based superconductors. *Nature Physics*, 18(12):1412–1419, 2022.
 [4] Minseok Choi, Fumiyasu Oba, Yu Kumagai, and Isao Tanaka. Anti-ferrodistortive-like oxygen-octahedron rotation induced by the oxygen vacancy in cubic srtio3. *Advanced Materials*

- (Deerfield Beach, Fla.), 25(1):86–90, 2012.
- [5] Aylin M Deliormanli, Shams AM Issa, MS Al-Buriahi, Begüm Rahman, Hesham MH Zakaly, and HO Tekin. Erbium (iii)-and terbium (iii)-containing silicate-based bioactive glass powders: Physical, structural and nuclear radiation shielding characteristics. *Applied Physics A*, 127(6):463, 2021.
- [6] Hao Ding, Yan-Feng Lv, Kun Zhao, Wen-Lin Wang, Lili Wang, Can-Li Song, Xi Chen, Xu-Cun Ma, and Qi-Kun Xue. High-temperature superconductivity in single-unit-cell fese films on anatase tio₂ (001). *Physical review letters*, 117(6):067001, 2016.
- [7] Brendan D Faeth, Saien Xie, Shulong Yang, Jason K Kawasaki, Jocienne N Nelson, Shuyuan Zhang, Christopher Parzyck, Pramita Mishra, Chen Li, Christopher Jozwiak, et al. Interfacial electron-phonon coupling constants extracted from intrinsic replica bands in monolayer fese/srtio₃. *Physical review letters*, 127(1):016803, 2021.
- [8] Guanming Gong, Haohao Yang, Qinghua Zhang, Cui Ding, Jingsong Zhou, Yujie Chen, Fanqi Meng, Zhiyu Zhang, Wenfeng Dong, Fawei Zheng, et al. Oxygen vacancy modulated superconductivity in monolayer fese on srtio₃- δ . *Physical Review B*, 100(22):224504, 2019.
- [9] JH Haeni, Chris D Theis, and Darrell G Schlom. Rheed intensity oscillations for the stoichiometric growth of srtio₃ thin films by reactive molecular beam epitaxy. *Journal of Electroceramics*, 4:385–391, 2000.
- [10] Shaolong He, Junfeng He, Wenhao Zhang, Lin Zhao, Defa Liu, Xu Liu, Daixiang Mou, Yun-Bo Ou, Qing-Yan Wang, Zhi Li, et al. Phase diagram and electronic indication of high-temperature superconductivity at 65 k in single-layer fese films. *Nature materials*, 12(7):605–610, 2013.
- [11] PJ Hirschfeld, MM Korshunov, and II Mazin. Gap symmetry and structure of fe-based superconductors. *Reports on Progress in Physics*, 74(12):124508, 2011.
- [12] Caiyun Hong, Zhen Song, Bing Lin, Pengxu Ran, Xiaopeng Xie, Congying Jiang, and Rui-Hua He. Effect of surface reconstruction of srtio₃ (001) on the fese thin film growth. *Journal of Physics and Chemistry of Solids*, 184:111717, 2024.
- [13] Fong-Chi Hsu, Jiu-Yong Luo, Kuo-Wei Yeh, Ta-Kun Chen, Tzu-Wen Huang, Phillip M Wu, Yong-Chi Lee, Yi-Lin Huang, Yan-Yi Chu, Der-Chung Yan, et al. Superconductivity in the pbo-type structure α -fese. *Proceedings of the National Academy of Sciences*, 105(38):14262–14264, 2008.
- [14] Tao Jia, Zhuoyu Chen, Slavko N Rebec, Makoto Hashimoto, Donghui Lu, Thomas P Devereaux, Dung-Hai Lee, Robert G Moore, and Zhi-Xun Shen. Magic doping and robust superconductivity in monolayer fese on titanates. *Advanced Science*, 8(9):2003454, 2021.
- [15] Mohamed Ali Khaled, Juan Ruvalcaba, T Fraga Córdova, Mimoun El Marssi, and Houssny Bouyanfif. Spin-lattice coupling in an epitaxial ndfeo₃ thin film. *Materials Letters*, 309:131442, 2022.
- [16] Mohamed Ali Khaled, Juan Ruvalcaba, T Cordova-Fraga, Donna C Arnold, Nicolas Jaouen, Philippe Ohresser, Mustapha Jouiad, Khalid Hoummada, Brahim Dkhil, Mimoun El Marssi, et al. Strain engineering of the magnetic anisotropy and magnetic moment in ndfeo₃ epitaxial thin films. *Physical Review Materials*, 6(6):064412, 2022.
- [17] WC Koehler, EO Wollan, and MK Wilkinson. Neutron diffraction study of the magnetic properties of rare-earth-iron perovskites. *Physical Review*, 118(1):58, 1960.
- [18] JJ Lee, FT Schmitt, RG Moore, S Johnston, Y-T Cui, W Li, M Yi, ZK Liu, M Hashimoto, Ya Zhang, et al. Interfacial mode coupling as the origin of the enhancement of t_c in fese films on srtio₃. *Nature*, 515(7526):245–248, 2014.
- [19] Fengmiao Li, Ilya Elfmov, and George A Sawatzky. Modulation doping of the fese monolayer on srtio₃. *Physical Review B*, 105(21):214518, 2022.
- [20] Fengmiao Li and George A Sawatzky. Electron phonon coupling versus photoelectron energy loss at the origin of replica bands in photoemission of fese on srtio₃. *Physical Review Letters*, 120(23):237001, 2018.
- [21] Wei Li, Yan Zhang, Peng Deng, Zhilin Xu, S-K Mo, Ming Yi, Hao Ding, M Hashimoto, RG Moore, D-H Lu, et al. Stripes developed at the strong limit of nematicity in fese film. *Nature Physics*, 13(10):957–961, 2017.
- [22] Chong Liu, Hyunki Shin, Andrin Doll, Hsiang-Hsi Kung, Ryan P Day, Bruce A Davidson, Jan Dreiser, Giorgio Levy, Andrea Damascelli, Cinthia Piamonteze, et al. High-temperature superconductivity and its robustness against magnetic polarization in monolayer fese on eutio₃. *npj Quantum Materials*, 6(1):85, 2021.
- [23] Worawat Meevasana, PDC King, RH He, SK Mo, M Hashimoto, Anna Tamai, P Songsiririthigul, Félix Baumberger, and ZX Shen. Creation and control of a two-dimensional electron liquid at the bare srtio₃ surface. *Nature materials*, 10(2):114–118, 2011.
- [24] Y Miyata, K Nakayama, K Sugawara, T Sato, and T Takahashi. High-temperature superconductivity in potassium-coated multilayer fese thin films. *Nature materials*, 14(8):775–779, 2015.
- [25] K Nakayama, Y Miyata, GN Phan, T Sato, Y Tanabe, T Urata, K Tanigaki, and T Takahashi. Reconstruction of band structure induced by electronic nematicity in an fese superconductor. *Physical review letters*, 113(23):237001, 2014.
- [26] Dushyant M Narayan, Peipei Hao, Rafał Kurlito, Bryan S Berggren, A Garrison Linn, Christopher Eckberg, Pratham Saraf, John Collini, Peter Zavalij, Makoto Hashimoto, et al. Potential lifshitz transition at optimal substitution in nematic pnictide ba_{1-x}sr_xni₂as₂. *Science Advances*, 9(42):ead4966, 2023.
- [27] Samantha O’Sullivan, Ruizhe Kang, Jules A Gardener, Austin J Akey, Christian E Matt, and Jennifer E Hoffman. Imaging se diffusion across the fese/srtio₃ interface. *Physical Review B*, 105(16):165407, 2022.
- [28] R Peng, XP Shen, X Xie, HC Xu, SY Tan, M Xia, T Zhang, HY Cao, XG Gong, JP Hu, et al. Measurement of an enhanced superconducting phase and a pronounced anisotropy of the energy gap of a strained fese single layer in fese/nb: Srtio₃/ktao₃ heterostructures using photoemission spectroscopy. *Physical review letters*, 112(10):107001, 2014.
- [29] R Peng, HC Xu, SY Tan, HY Cao, M Xia, XP Shen, ZC Huang, CHP Wen, Q Song, T Zhang, et al. Tuning the band structure and superconductivity in single-layer fese by interface engineering. *Nature communications*, 5(1):5044, 2014.
- [30] GN Phan, K Nakayama, K Sugawara, T Sato, T Urata, Y Tanabe, K Tanigaki, F Nabeshima, Y Imai, A Maeda, et al. Effects of strain on the electronic structure, superconductivity, and nematicity in fese studied by angle-resolved photoemission spectroscopy. *Physical Review B*, 95(22):224507, 2017.
- [31] R Przeniosło, I Sosnowska, and B Frick. Nuclear ordering and excitations in ndfeo₃. *Journal of magnetism and magnetic materials*, 305(1):186–190, 2006.
- [32] SN Rebec, T Jia, C Zhang, M Hashimoto, D-H Lu, RG Moore, and Z-X Shen. Coexistence of replica bands and superconductivity in fese monolayer films. *Physical review letters*, 118(6):067002, 2017.
- [33] Luke C Rhodes, Matthias Eschrig, Timur K Kim, and Matthew D Watson. Fese and the missing electron pocket prob-

- lem. *Frontiers in Physics*, 10:243, 2022.
- [34] Jonathan A Sobota, Yu He, and Zhi-Xun Shen. Angle-resolved photoemission studies of quantum materials. *Reviews of Modern Physics*, 93(2):025006, 2021.
- [35] Can-Li Song, Hui-Min Zhang, Yong Zhong, Xiao-Peng Hu, Shuai-Hua Ji, Lili Wang, Ke He, Xu-Cun Ma, and Qi-Kun Xue. Observation of double-dome superconductivity in potassium-doped fese thin films. *Physical review letters*, 116(15):157001, 2016.
- [36] Qi Song, TL Yu, Xia Lou, BP Xie, HC Xu, CHP Wen, Q Yao, SY Zhang, XT Zhu, JD Guo, et al. Evidence of cooperative effect on the enhanced superconducting transition temperature at the fese/srtio3 interface. *Nature communications*, 10(1):758, 2019.
- [37] Yuanhe Song, Zheng Chen, Qinghua Zhang, Haichao Xu, Xia Lou, Xiaoyang Chen, Xiaofeng Xu, Xuetao Zhu, Ran Tao, Tianlun Yu, et al. High temperature superconductivity at fese/lafeo3 interface. *Nature Communications*, 12(1):5926, 2021.
- [38] I Sosnowsk, E Steichelea, and A Hewatc. Reorientation phase transition in ndfeo 3. *Physica B+ C*, 136(1):394–396, 1986.
- [39] Shiyong Tan, Yan Zhang, Miao Xia, Zirong Ye, Fei Chen, Xin Xie, Rui Peng, Difei Xu, Qin Fan, Haichao Xu, et al. Interface-induced superconductivity and strain-dependent spin density waves in fese/srtio3 thin films. *Nature materials*, 12(7):634–640, 2013.
- [40] Chenjia Tang, Chong Liu, Guanyu Zhou, Fangsen Li, Hao Ding, Zhi Li, Ding Zhang, Zheng Li, Canli Song, Shuaihua Ji, et al. Interface-enhanced electron-phonon coupling and high-temperature superconductivity in potassium-coated ultrathin fese films on srtio 3. *Physical Review B*, 93(2):020507, 2016.
- [41] D Treves. Studies on orthoferrites at the weizmann institute of science. *Journal of Applied Physics*, 36(3):1033–1039, 1965.
- [42] Qing-Yan Wang, Zhi Li, Wen-Hao Zhang, Zuo-Cheng Zhang, Jin-Song Zhang, Wei Li, Hao Ding, Yun-Bo Ou, Peng Deng, Kai Chang, et al. Interface-induced high-temperature superconductivity in single unit-cell fese films on srtio3. *Chinese Physics Letters*, 29(3):037402, 2012.
- [43] Qisi Wang, Yao Shen, Bingying Pan, Yiqing Hao, Mingwei Ma, Fang Zhou, P Steffens, Karin Schmalzl, TR Forrest, Mahmoud Abdel-Hafiez, et al. Strong interplay between stripe spin fluctuations, nematicity and superconductivity in fese. *Nature materials*, 15(2):159–163, 2016.
- [44] CHP Wen, HC Xu, Chen Chen, ZC Huang, Xia Lou, YJ Pu, Qi Song, BP Xie, Mahmoud Abdel-Hafiez, DA Chareev, et al. Anomalous correlation effects and unique phase diagram of electron-doped fese revealed by photoemission spectroscopy. *Nature communications*, 7(1):10840, 2016.
- [45] Ming Yi, Heike Pfau, Yan Zhang, Yu He, Han Wu, Tong Chen, ZR Ye, Makoto Hashimoto, Rong Yu, Qimiao Si, et al. Nematic energy scale and the missing electron pocket in fese. *Physical Review X*, 9(4):041049, 2019.
- [46] Chaofan Zhang, Zhongkai Liu, Zhuoyu Chen, Yanwu Xie, Ruihua He, Shujie Tang, Junfeng He, Wei Li, Tao Jia, Slavko N Rebec, et al. Ubiquitous strong electron–phonon coupling at the interface of fese/srtio3. *Nature communications*, 8(1):14468, 2017.
- [47] Huimin Zhang, Ding Zhang, Xiaowei Lu, Chong Liu, Guanyu Zhou, Xucun Ma, Lili Wang, Peng Jiang, Qi-Kun Xue, and Xinhe Bao. Origin of charge transfer and enhanced electron–phonon coupling in single unit-cell fese films on srtio3. *Nature Communications*, 8(1):214, 2017.
- [48] P Zhang, X-L Peng, T Qian, P Richard, X Shi, J-Z Ma, BB Fu, Y-L Guo, ZQ Han, SC Wang, et al. Observation of high- t_c superconductivity in rectangular fese/srtio 3 (110) monolayers. *Physical Review B*, 94(10):104510, 2016.
- [49] Peng Zhang, T Qian, P Richard, XP Wang, H Miao, BQ Lv, BB Fu, T Wolf, C Meingast, XX Wu, et al. Observation of two distinct d_xz/d_yz band splittings in fese. *Physical Review B*, 91(21):214503, 2015.
- [50] WH Zhang, X Liu, CHP Wen, R Peng, SY Tan, BP Xie, T Zhang, and DL Feng. Effects of surface electron doping and substrate on the superconductivity of epitaxial fese films. *Nano letters*, 16(3):1969–1973, 2016.
- [51] Y Zhang, M Yi, Z-K Liu, W Li, JJ Lee, RG Moore, M Hashimoto, M Nakajima, H Eisaki, S-K Mo, et al. Distinctive orbital anisotropy observed in the nematic state of a fese thin film. *Physical Review B*, 94(11):115153, 2016.
- [52] Guanyu Zhou, Ding Zhang, Chong Liu, Chenjia Tang, Xiaoxiao Wang, Zheng Li, Canli Song, Shuaihua Ji, Ke He, Lili Wang, et al. Interface induced high temperature superconductivity in single unit-cell fese on srtio3 (110). *Applied Physics Letters*, 108(20), 2016.
- [53] Yong Hu, Yu Xu, Qingyan Wang, Lin Zhao, Shaolong He, Jianwei Huang, Cong Li, Guodong Liu, and XJ Zhou. Identification of a large amount of excess fe in superconducting single-layer fese/srtio 3 films. *Physical Review B*, 97(22):224512, 2018.